2023

Analysis of Laminar Flow Patterns in Milifluidic Devices

Brian Leger

Analysis of Laminar Flow Patterns in Millifluidic Devices

Brian Leger

Faculty Mentor:

Benjamin J. Knurr, Ph.D.

Assumption University

College of Liberal Arts and Sciences

Department of Biological and Physical Sciences

A thesis submitted to fulfill the requirements of
the honors program at Assumption University

Fall 2023

Abstract

This research centers around a millifluidic device designed for the analysis of flowing chemical reactions that may happen too quickly to be analyzed by traditional spectroscopic methods. The device works by combining two simple concepts: fluid flows a certain distance over time and chemical reactions progress over time. Combining these allows for the correlation of reaction progress and distance through the device. Since the flow within the device is laminar, there is friction along the walls of the channel that creates a flow profile that elongates over time. The details of the flow were previously unknown but are necessary if the device is to be used for future chemical kinetics research. This paper studies the nature of the flow by creating a simulation and an experiment to measure the laminar flow head. A spectroscopy calculator program was created to accompany the device that allows for an accurate prediction of spectral data to be collected using the device. The work presented here will be used to guide future experiment choices for these millifulidic devices.

Acknowledgements

Special acknowledgements go to the faculty of Assumption University, especially Dr. Benjamin Knurr, Dr. Molly McGrath, Dr. Elizabeth Colby Davie, and Dr. Maria Teresa Herd. Heartfelt thanks go out to my friends and family, especially my girlfriend as well as my dad, for their many hours spent listening to explanations, encouragement through late night writing, and proofreading this paper.

1 - Intro

Once a chemical reaction is started there is virtually no way to freeze it in time, the reaction will continue to progress, some slowly and some very quickly. While spectroscopic studies are often used to analyze the reactants and products present in a reaction mixture, it can be difficult to perform these experiments or they may generate inconclusive results if done while the reaction is actively progressing. There may be no way to truly stop a reaction once started but there is a way to analyze it using a simple physics principle. Velocity is change in position over time and a chemical reaction progresses over time. Combining the two can solve the problem of analyzing a reaction that is progressing. This simple equation shows how time can be correlated to distance:

$$\frac{Distance}{Velocity} = Time$$

By flowing the reacting mixture such that a spectroscope can measure the reaction at a certain position along the flow path, the reaction can be observed at a specific time in its progress. One such reaction that could benefit from additional study of a progressing reaction is the formation of the iodine starch complex as the secondary reaction or reactions remains a mystery to chemists. The reactants are known, but the reaction kinetics and structure of the product complex are still not known even after over 100 years of study.

This connection between time, distance, and velocity is the basic concept by which the millifluidic device being studied functions. Designed by Dr. Benjamin Knurr and Sarah Morley (Assumption class of 2018), the 2 by 3 inch device [2] allows for the study the reaction kinetics of and chemical species present in various chemical reactions. The device has two inputs to attach syringe pumps for two separate fluids. The fluids enter the device then go through a pseudo-helical

static mixing region which completely homogenizes the liquids. The now reacting fluid flows through a 1.5 mm^2 square, 372.5 mm long channel and out into a waste container. While moving through the device, the fluid exhibits a laminar flow, allowing for the tracking of particles through the device.

The flow in this device had to be carefully studied. Because it was laminar, the velocity of the flow was not the same across the width of the channel. Friction along the walls of the channel made the flow along the edges slow down relative to the center velocity. Simulations in FLOW-3D [2] agreed with this expectation. The simulations also showed that the flow velocities not only differed across the width of the channel but also exhibited a consistent elliptical paraboloid shape. The simulations also predicted that this shape elongated as the flow progressed through the device. This results in multiple velocities, and thus reaction times, being measured simultaneously. For chemical kinetic information to be obtained from the acquired spectra, a complete understanding of the velocities present is required.

After simulating flow within the device, a physical experiment had to be designed that allowed for the verification of the simulated model. Dye was injected into one of the inputs of the device that allowed for the tracking of the shape of the flow head. Data was then collected from the physical experiment using a video of the flow within the device and the industry standard image analysis program, ImageJ. The width of the flow head was measured at various points along the length of the channel. This was then formed into a table of the relative velocity distribution over the width of a cross-section of the channel.

Using the velocity distribution, a spectroscopy simulator was developed. Because initial data from the testing of the device was spectroscopic, the simulated data had to be comparable

with the previously collected experimental data to validate the flow model. This involved using the equation of the relationship between velocity, distance, and reaction progress (time).

2 - History and Previous Research

The millifluidic device being studied in this project was designed by Dr. Benjamin Knurr and Sarah Morley for use in chemical reaction analysis. Physical chemists are often interested in reaction kinematics, or how a reaction happens on a molecular level. The device is designed to allow chemists to study a reaction while it is in the process of reacting. The device has two inputs for constantly flowing liquid reactants, which allows a chemical reaction to happen as the liquid is flowing. This is the key principle on which the device operates. Reactions happen over time and flowing liquid changes position over time, therefore the position and elapsed time of reaction can be correlated. At a specific point in the device, the reaction can be predicted to be at a certain time through the reaction.

The device was designed to be used to study any number of chemical reactions and modified for other purposes as well. The formation of the iodine-starch complex, commonly observed in iodine clock reactions, is a chemical species whose structure has puzzled chemists for years. The reactants are known, but the process of the reaction and the exact structure and identity of the products are a mystery. Often, a good way to analyze a reaction is through spectroscopy, but an active reaction can only be analyzed for a very short amount of time due to the fact that the reaction is progressing while it is being measured. These devices allow for the analysis of a specific moment in the reaction for as long as is needed due to constantly flowing fresh reaction mixture.

During the initial research performed with the device, valuable information regarding the role of the solvent shell in influencing the properties of the iodine-starch complex was gained using the device. However, during the analysis it became clear that due to the nature of the different velocities present in the flow it was going to be very complicated to elicit kinetic information from

the acquired spectra. This realization was the impetus for the current study of the laminar flow dynamics present in the previously designed millifluidic devices.

3 - The Device and Its Purpose

The millifluidic device was designed around 2 by 3 inch quartz microscope slides to allow the reaction to be viewed from the top and bottom. The quartz is optically clear when viewed through a UV-Vis spectrometer making it an ideal choice for the covers. The base of the device is composed of 3D printed thermoplastic (usually ABS plastic), which allowed for the easy and rapid prototyping of the device. In addition, the chemicals being used could stain or damage the plastic, so it had to be potentially single use and therefore inexpensive and easy to make. The 3D printed plastic core was sandwiched between the two quartz slides using two-part epoxy for a complete seal. The inputs were designed so lure-lock millifluidic fittings could screw into the device. The other end of the input tubing was attached to a syringe on a syringe pump to allow for an extremely precise flow rate control.

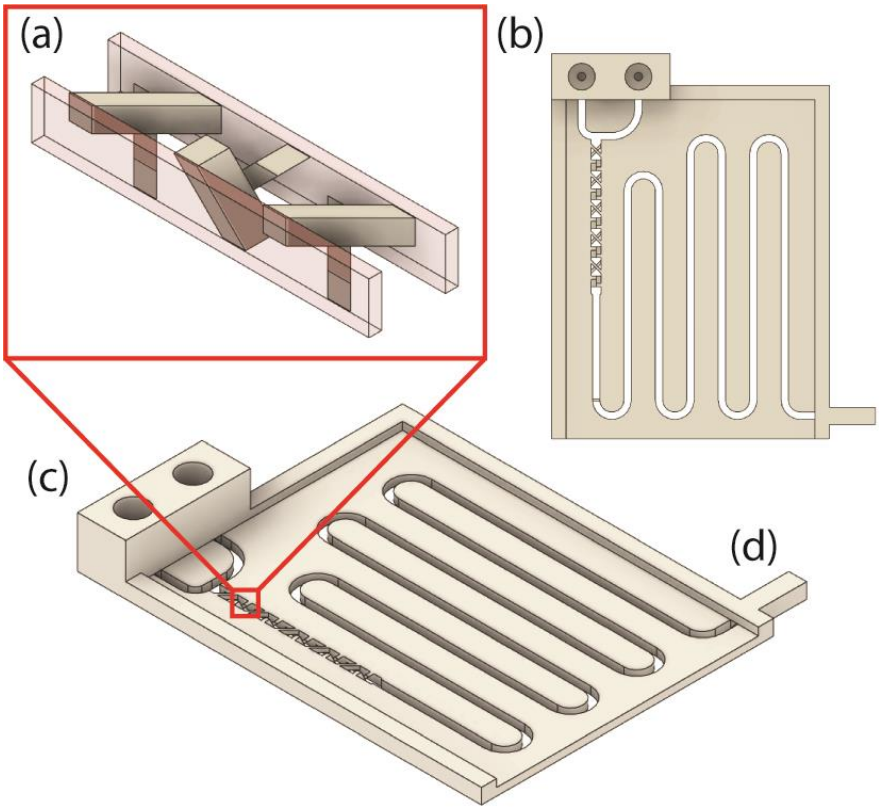

Figure 3.1: Diagram of the 3D printed plastic part of the device before being sandwiched with microscope slides. (a) shows a close-up of the pseudo-helical static mixing region, (b) shows the device when viewed from the top, (c) indicates the two fluid input holes, and (d) indicates where the fluid exits the device

Since the fluid flowing through the device is in a very small volume and at relatively slow speeds, the flow is considered laminar (not turbulent) and thus has a predictable velocity profile. This property of the flow was determined objectively using Reynolds number[3] calculations:

$$Re = \frac{\rho Q D_H}{\mu A}$$

where ρ is the density of the fluid, Q is the volumetric flow rate, D_H is the hydraulic diameter, μ is the dynamic viscosity, and A is the pipe's cross-sectional area.

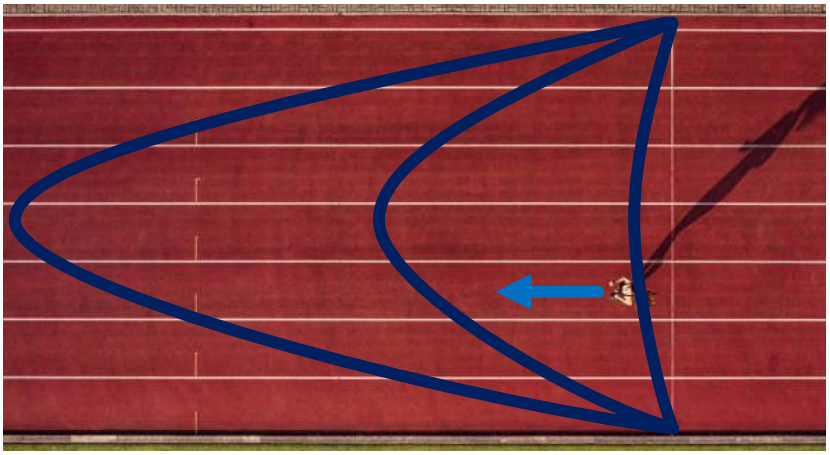

Figure 3.2: A visual representation of how particles of flow spread farther from each other like runners on a track. If each individual person maintains the same speed, the faster runners will get progressively further and further from the slower

If the Reynolds number of a flow is smaller (<2000), the flow is laminar, and if it is larger (>2000), the flow is more turbulent. The number representing the flow in the device was found to have an extremely small number, indicating that the flow was laminar. The Reynolds number of the flow within the device was found to be approximately 3.

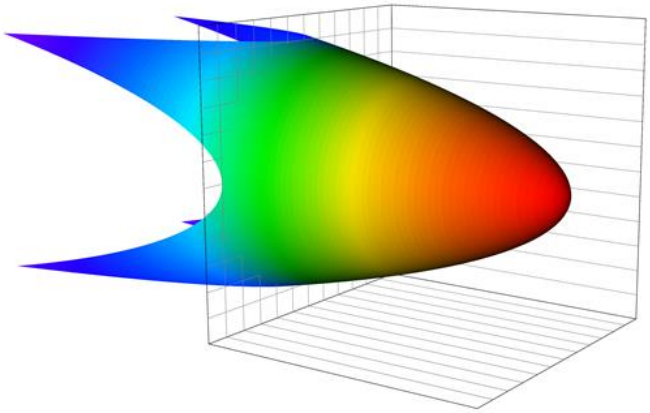

Figure 3.3: A rendered image of an elliptical paraboloid representing the shape that the flow head takes on as it moves down the channel. In the experiment, the flow head is much longer, but this rendering has been shortened for ease of viewing.

"Laminar flow" means that any given particle of the fluid is flowing in the exact same direction as another in its flow plane, but not necessarily at the same speed. Particles toward the center of the flow volume move

faster than those near the walls. This discrepancy in speed results in a distribution of velocities rather than the entire fluid moving at one speed. This project is centered around the study of the speed of fluid flow through different areas of the device and how understanding and seeing if modeling the distribution of speeds can be used to acquire reaction kinetics data.

To visualize the effect of laminar flow, think of the flow in the channels as athletes running a race (Figure 3.1). They start at the same line. Imagine the people in the middle lanes run faster than those in the outer lanes. As they get further down the track, the faster runners move progressively further and further away from the others. The same principle applies for the flow within the channels. The particles of fluid in the center of the flow volume get progressively further and further along the flow path much faster than the particles on the outside of the channel.

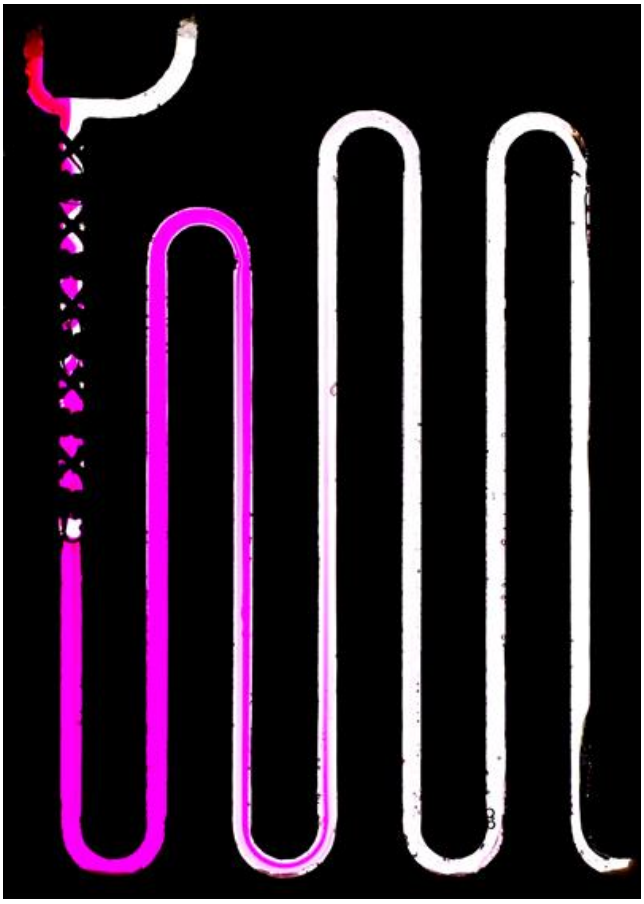

Figure 3.4: A high-resolution picture of the flow head spanning from channel two to channel four. (approximately 2.5 channels in length)

It is known that liquid moves slower along the sides of a channel (aka a pipe or a duct) and faster in the center. Friction from the channel walls causes the fluid to slow and, due to this friction, it can be observed that fluid on the sides will have a slower rate of flow than fluid in the middle. Essentially, if you observe a cross-section of the flow immediately after the mixing region, where laminar flow begins, it will elongate from a flat plane to a roughly bullet-shaped cone. This shape is formally known as

an elliptical paraboloid (Figure 3.3). This paraboloid shape will get longer and longer as liquid flows through the device. The precise rate of elongation (curvature of the paraboloid) can be found if one precisely determines the rates of flow at given points in the device.

One purpose of this device is to observe reaction progress over time based on the distance the fluid has traveled. Since this device is intended to be used in chemical reaction analysis, so it is useful to know how long the liquids have been reacting. If two reactants are input at the same rate, they will enter the device and start reacting as they flow together. As previously discussed, the flow rate is different in different areas of the channel cross-section. This means that the reaction in the middle of the channel will not be as advanced (shorter elapsed reaction time) as it is along the edges of the channel (longer elapsed time). The fluid on the edges of the channel spends more time in the device than the fluid in the center.

Chemical kinetics is the study of rates of reactions and the mechanisms that result in the generation of products from reactants. Necessarily, the study of kinetics often requires temporal information about the reaction taking place. For this reason, understanding the flow rate is crucial to the application of this device within the realm of chemical kinetics.

4 - Flow Simulations

The fluid dynamic simulation program FLOW-3D was used for all flow simulations in this study. It is an industry standard for any computational fluid dynamics analysis from groundwater filtration to disease transmission through air.

The previously designed 3D model of the device was first imported into FLOW-3D, after which the next step was to set various parameters with which the program could calculate the fluid dynamics analysis. These parameters included the input and output locations on the device, what fluid was being modeled, what material the device was made of, whether gravity affects the flow, and what is the boundary condition along the walls of the ducts.

The input and output had to be added to the 3D model to tell the program where to simulate the flow. The input was set to be a constant flow emanating from a plane surface that was perpendicular to the input channels of the device. The output was set to have no restriction. In other words, the simulated fluid vanished when it passed through the output plane.

Boundary conditions tell the program how to simulate flow in relation to the flow path in the model. The whole device was specified to be solid and made of plastic and the top and bottom were specified to be quartz. This reflected the real-world device that had been designed. However, it turned out that under the experimental flow conditions, the material choice did not dramatically affect the results. The next step was to determine whether the sides of the channel were a slip or no-slip condition. A no-slip boundary condition directs the program to set the velocity of the fluid touching the walls equal to 0 mm/s. A slip boundary assumes a certain level of movement along the walls (i.e., the velocity of the fluid touching the walls is greater than 0 mm/s). A no-slip boundary condition was chosen for the simulations because according to the principles of fluid

dynamics, as the flow approaches the walls of the channel, the velocity will approach 0 mm/s. Later in the project, this assumption turned out to be a potential problem as actual experimentation showed that the device with flowing water does not exhibit the ideal no-slip flow boundary conditions. However, specifying a no-slip boundary condition would have added a lot of extra computation time to complete the simulations. Since the license for FLOW-3D was only valid for the 2021 summer it was decided that keeping the simulations as simple and straightforward as possible was the most prudent decision.

The next element of the simulations that had to be determined was the mesh size. Computer simulations use a mesh or 3D cubic point cloud to specify where each particle/velocity will be calculated. The simulation cannot calculate every particle within a space down to an infinite granularity (trying to do so would take an infinite amount of time), so the mesh size sets the granularity of the calculation to provide a balance between computational limitations and simulation accuracy. At each cube in the mesh, FLOW-3D calculates the velocity vector of the particle for every set time increment. After running initial trials, it was realized that the size of the mesh had to be carefully determined and aligned so it would not intersect the device at any point. In other words, the program would produce an incorrect output if the mesh cube contained half plastic and half water. The output velocity vector would be zero because there was no water flowing through the device. To avoid this, the mesh had to be properly aligned within the model and the mesh size had to be a factor of the width of the square channel (1.5 mm).

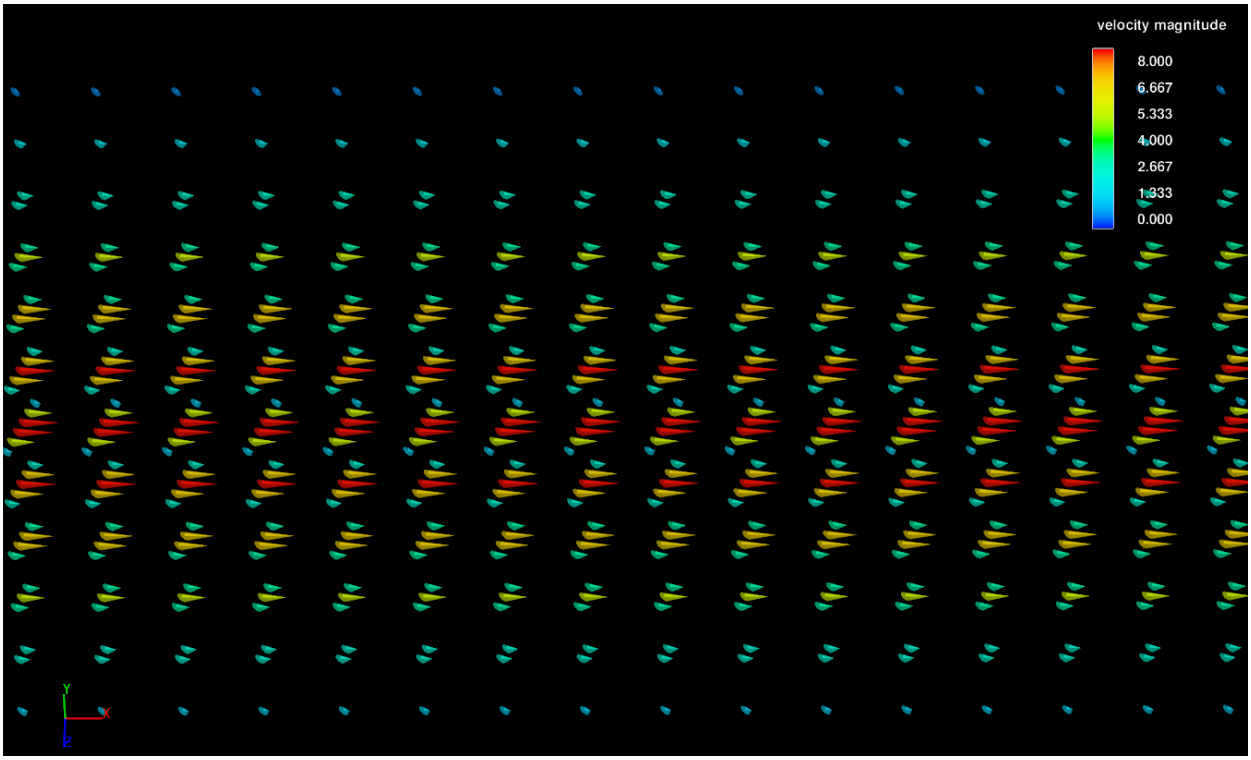

Figure 4.1: An enlarged view of a straight section of channel rendered with FLOW-3D showing the simulated velocity vectors represented with arrows whose length and color represents their magnitude. Red arrows indicate faster velocity and blue indicates slower velocity. Notice the mesh size is large and does not have a high granularity with only 12 mesh cells in each cross-sectional direction (height and width).

Another necessary consideration was that decreasing the mesh size (increasing the precision of the calculation) made the program take longer to complete the simulation. In other words, a finer mesh made simulations take longer. The time it took to run various simulations increased by the cube of the mesh size. For example, a volume of 20 mm^3 with a mesh size of 1 mm^3 represents 20 x 20 x 20 mesh points, which requires 8,000 calculations. Decreasing the mesh size to 0.1 mm^3 means that there will be 200 x 200 x 200 points and 8,000,000 calculations. Initial simulations were run at a mesh size of 0.1 mm^3 and took from 30 seconds to a few minutes. Later simulations, with a mesh size of 0.025 mm^3, took upwards of 2.5 weeks to calculate.

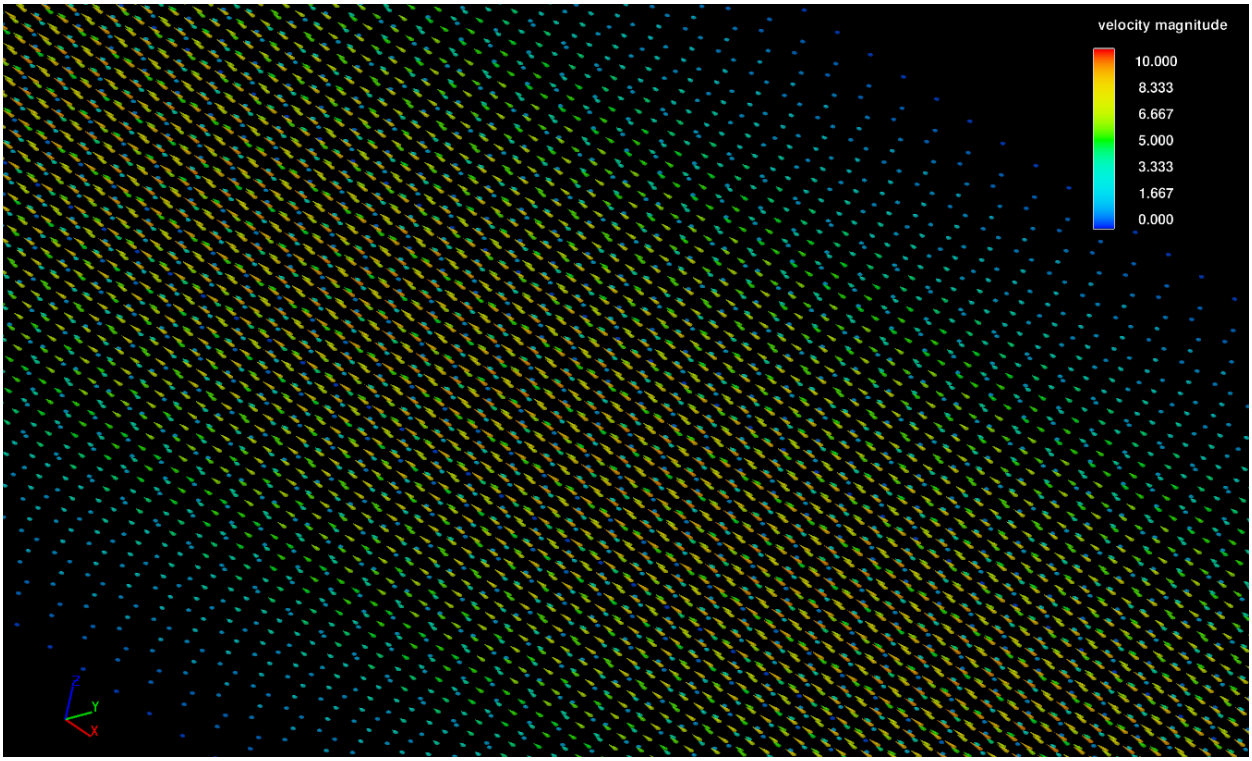

Figure 4.2: A view of a straight section of channel in the device rendered with FLOW-3D showing the resolution of a 0.025 mm^3 mesh. A cross-section of the velocities shown here is a 61x61 array.

Through the process of learning how to adjust the parameters of FLOW-3D, many simulations were run. An initial test of a short, straight section of channel was run to determine boundary conditions and input parameters. Flow in a longer section using a smaller mesh was then simulated to determine whether the flow was laminar down a channel. It was found to be laminar and it was confirmed that the velocities varied proportionally to the distance from the edges of the channel in the predicted elliptical paraboloid shape. A test was run of the curved section at the ends of the straight channel and confirmed that the flow remained laminar while flowing around the 180° curve of the device (see Figure 4.4).

A simulation with an extremely small mesh was run on the pseudo-helical static mixing region of the device. Marker particles, visually trackable particles with no simulated mass or volume, were added to trace the path of flow. The marker particles were added to one of the two

inputs of the device. A visual inspection of the channel at the output of the mixing region confirmed that it completely homogenized the liquid from the two inputs. This was an important

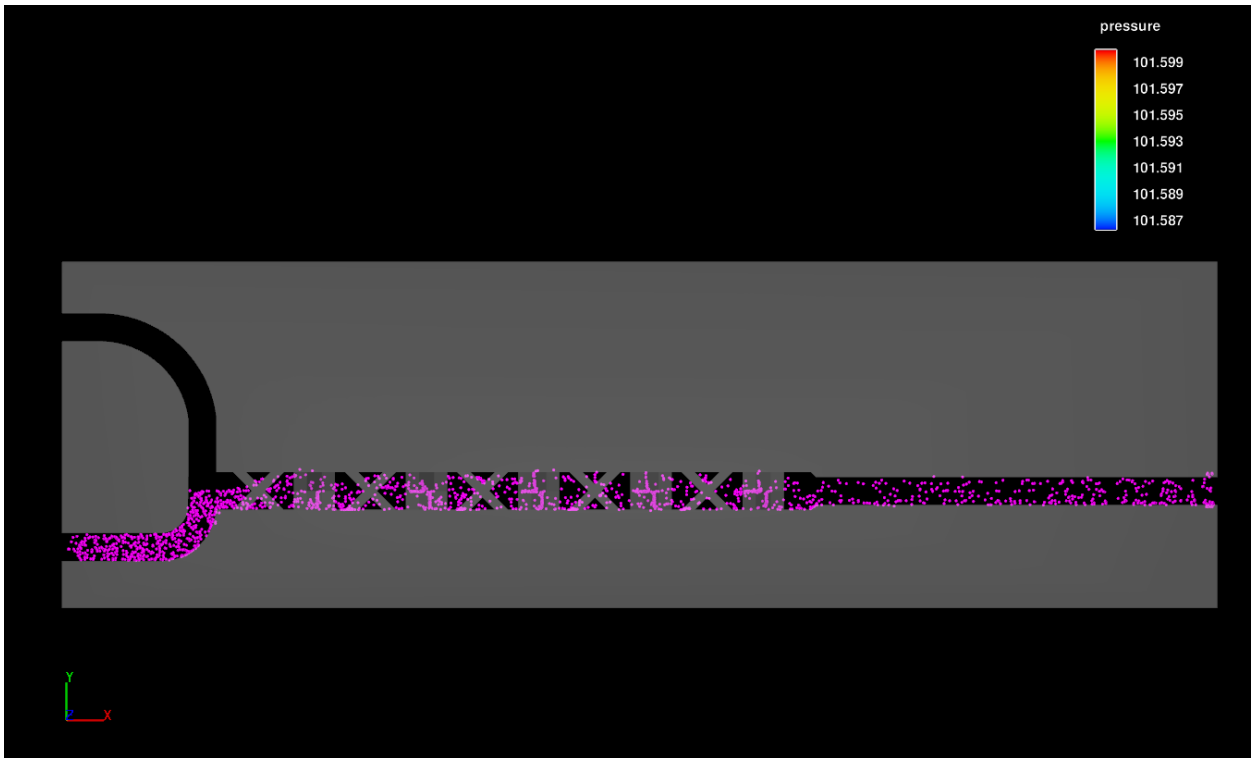

Figure 4.3: A top-down view of the mixing region rendered with FLOW-3D using pink marker particles to track the homogenization of the two input liquids.

test to confirm the effectiveness of the design of the pseudo-helical static mixer before moving forward with further tests.

Finally, a large simulation of the entire device was run with an extremely small mesh size of 0.025^3 mm^3. This simulation took about 2.5 weeks to run due to the mesh precision and size of the simulated area.

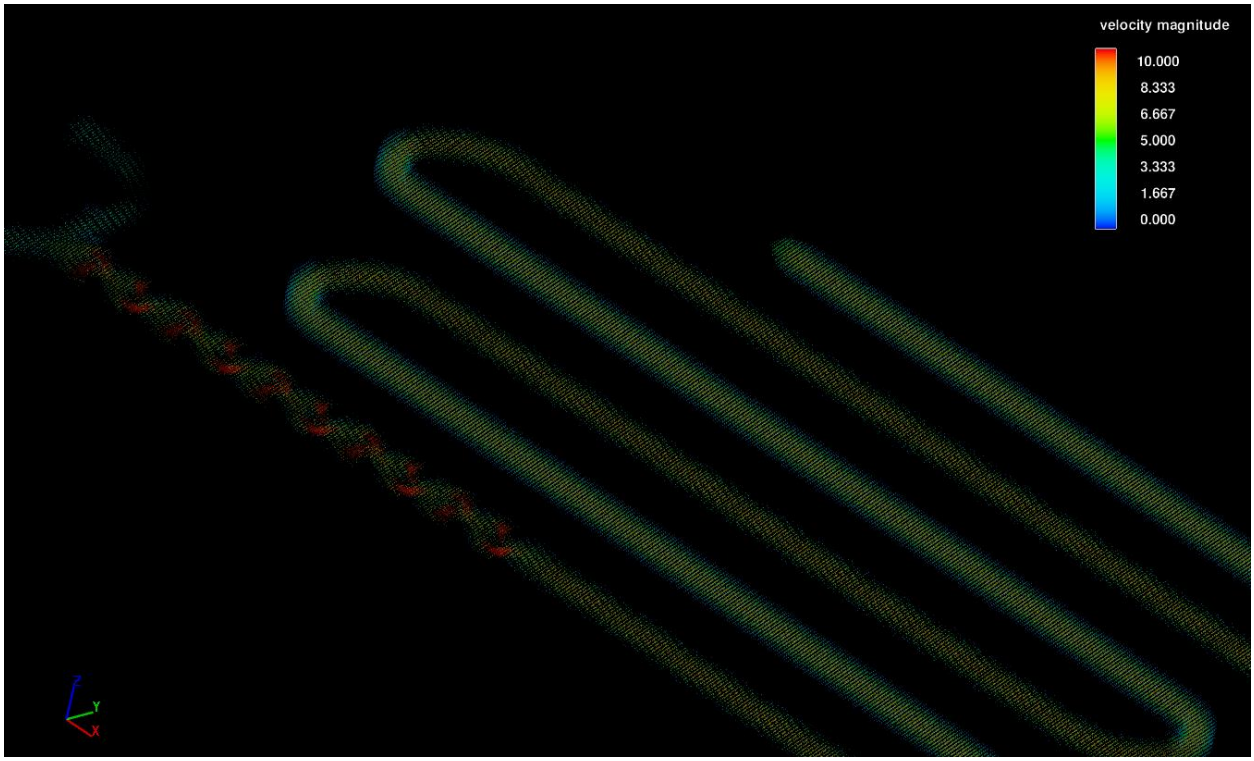

Figure 4.4: A zoomed out view of the velocity vectors for a simulation of the whole device rendered with FLOW-3D.

FLOW-3D rendered models of the flow that allowed the simulations to be visually confirmed, but precise numerical data was needed to graph the suspected flow head and offer a comparison for experimental data. The program output the data of each mesh cell to a text file. It made columns for the cell's position, the velocity of the particle, and the position of the particle in cartesian coordinate space. It produced a file that contained 6 columns (x, y, z positions and u (x), v (y), w (z) velocity vectors) with a row for each mesh cell. Since only the velocity in the x direction (direction of flow) mattered, only the x, y, z, and u data points were used. This data was then input into Microsoft Excel and graphed. The graph confirmed the elliptical paraboloid shape that was expected to form at a given square cross-section within the device, but the simulated results still needed to be tested against experimental data collected from the device.

5 - Experimental Procedure

a. Physical Setup

After simulating the flow, the next step was to design an experimental procedure by which the simulated flow patterns could be verified within the printed devices. The goal was to visualize and measure the profile of the suspected laminar flow planes, whether the mixing section successfully mixed the two input fluids, and if the channel walls exhibited no-slip or slip boundary conditions.

A setup was devised that allowed for the insertion of dye into a flow of water using a U6K Liquid Injector (used in high pressure liquid chromatography). This valve is unique because it allows a sample of a chemical to be input to the flow without stopping the flow to load the sample. The liquid injector was initially chosen because it allowed for a consistent amount of dye to be input every run. When the valve is switched from “test” to “load” the flow switches from a narrow diameter to a large diameter tubing. The reason for this switch is for the flow to take the path of

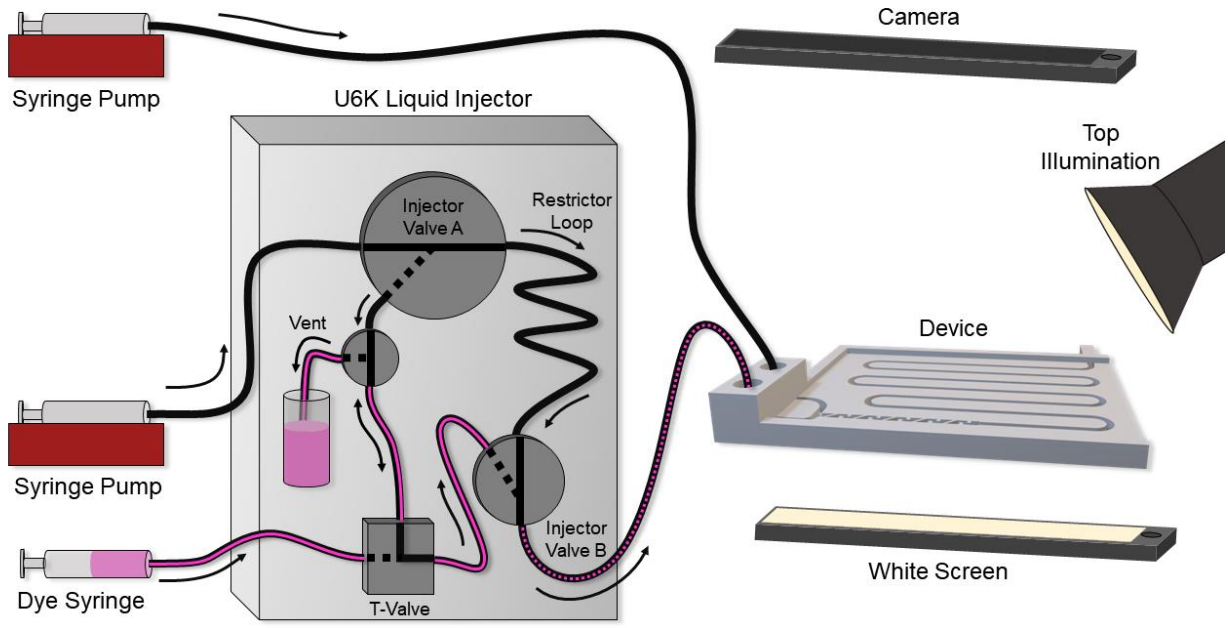

Figure 5.1: Experimental setup designed around the U6K liquid injector. Dotted lines indicate the secondary positions of the valves. All valves are turned momentarily to allow for dye loading then turned back to inject the dye into the device.

least resistance. While the flow diverts to the easiest path, the thinner tubing is available for the dye sample to be loaded. This method initially seemed the best because it allowed for an uninterrupted flow of liquid, but it was discovered that the change in diameter altered the flow rate and pressure in the device. There were two reasons the liquid system was not used for further testing. The change of diameter affected the flow more than anticipated and the liquid injector would often become clogged and would prevent the dye from flowing through and reaching the device thus ruining an experimental trial.

A new setup was then engineered and allowed for dye to be input from a loaded dye syringe while both pumps were still running. First the lever of injector had to be set to “load” to load the sample (dye). Next, it was turned to inject to inject the dye into the flow that went to the device. A T-valve was added outside the liquid injector between the dye syringe and the liquid injector so that pressure would not force clean water into the dye syringe instead of the device. However, this setup again suffered from clogs and leaks within the U6K Injector block so the entire U6K was removed from the experimental setup in favor of a simpler setup.

A similar design was created using only tubing of the same diameter, so as not to create different flow rates or pressures arising from the two pumps, and two T-valves used to create an input section with a vent. This allowed dye to be input, but it interrupted the flow to the device. The reason this was designed using two T-valves was to prevent air bubbles. If the tubing was disconnected and reconnected in adding a dye, it could allow air bubbles to form at the connection points, thus interrupting the flow and invalidating the test. It was found that this method did not affect flow or pressure because the flow had time to equalize while the fluid flowed through the approximately 2 ft of tubing on its way to the device. In addition, this only affected the flow to one

of the two inputs, so the flow did not completely stop in the device, but simply moved slower for a very short amount of time.

When dye was to be injected into the flow, the second pump was turned off very briefly to allow for the two T-valves to be set to the loading orientation. After dye was loaded and was flowing out of the vent port, the valves were then switched to allow the water to flow through to the device and the pump was turned back on. This whole process took a few seconds to perform and did not interrupt the flow enough for there to be any noticeable change in the flow data.

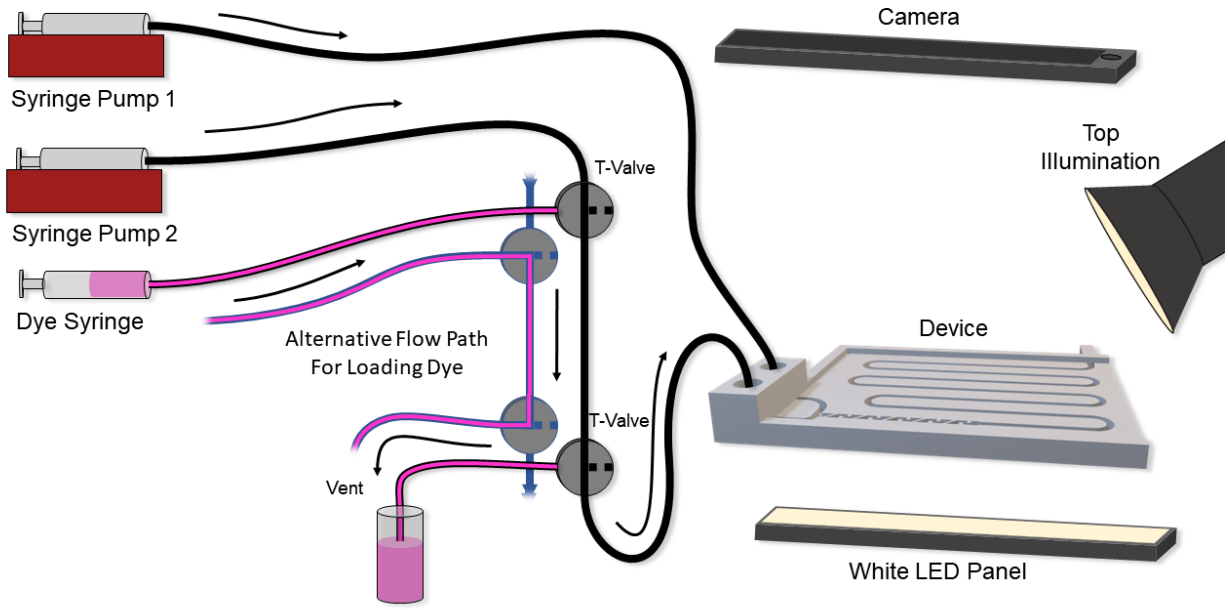

Figure 5.2: Experimental setup inspired by the U6K liquid injector design. It is based around two T-valves to allow for insertion of dye without the addition of bubbles. Both valves are momentarily turned and the dye syringe pushed to allow for the insertion of dye. During this moment (labeled "alternative flow path for loading dye" and outlined in blue), the dye flows from the syringe into the main tube and out into the vent (to prevent bubbles). The valves are then turned back to their normal position and the section between the two T-valves, now filled with dye, is pushed out to the device

Both experimental setups used an iPhone 12 Pro as the video recorder, a white LED backlight, and top illumination. The exact camera settings were changed from over many different trials to find the optimal settings for consistently detecting the difference between dye and the device walls.

It was found that a white LED backlight helped to illuminate the dye and increase contrast between the dye and the device. A white LED top light helped to illuminate the plastic device from the top to increase contrast and to compensate for the relatively dark device compared to the bright white background and pink glow of the backlit dye. Part-way through the project, it was found that green 3D-Printed devices produced a better contrast against the pink dye. This concept of color is discussed more in Section 5b.

To record video and still images of the flow within the device, a stand was designed to hold the device level with a specially designed phone holder above the device. The stand also held the light under the device. All were checked with a level before each run to ensure that there would be no camera lens distortion or light differences across the image that could add inconsistencies to the data.

b. Changes Made to Experimental Procedure Over Time

Throughout the course of studying the flow in the millifluidic device, many revisions were made to the experimental procedure. Changes were not made by category but are discussed in chronological order by category for ease of understanding. As was previously stated, the camera system on an iPhone 12 Pro was used for all videos, but settings were refined. This will be further discussed in Section 6.

Initially, the devices were 3D printed using white ABS plastic, but after many trials it was decided that a change in color to green would contrast against the pink dye better. Lighting was optimized through experimentation as well. It was determined that a white LED panel backlight under the device and a white led microscope lamp top light aided in contrast between the dye, empty channel, and device walls.

Dye

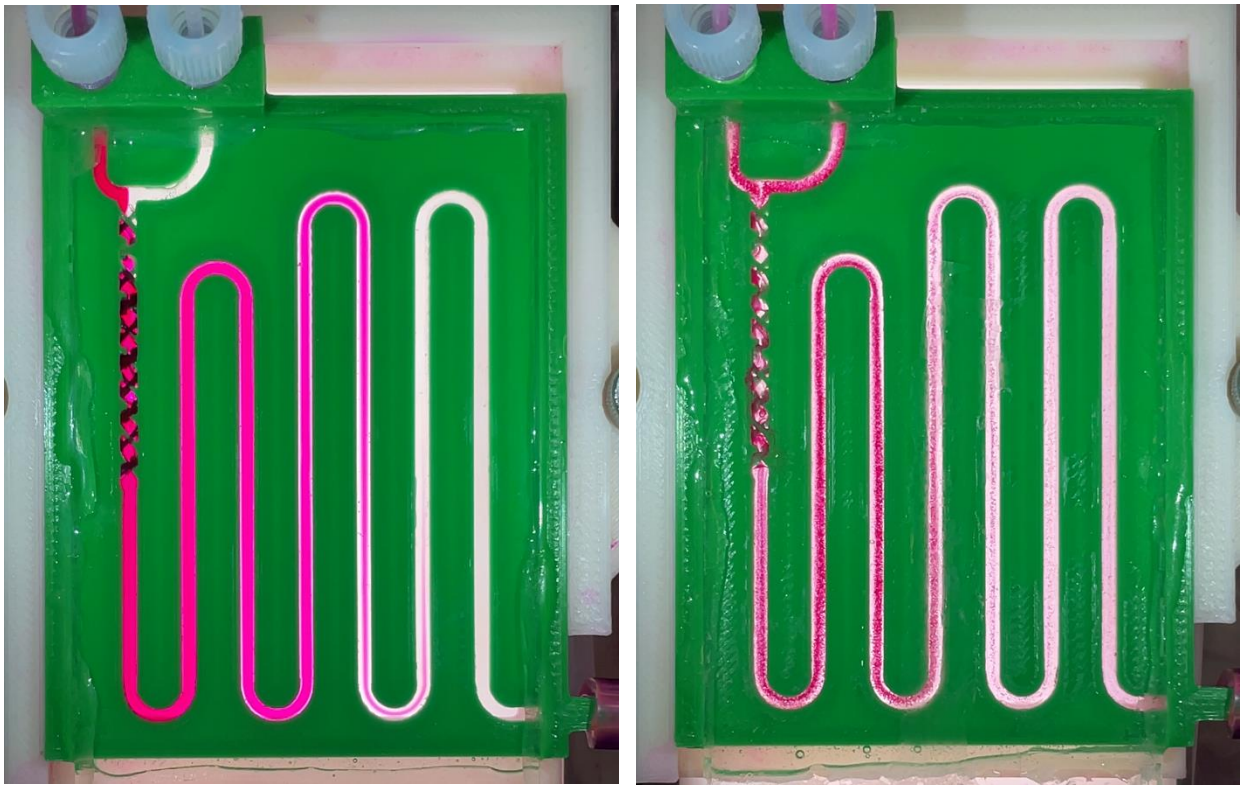

Figure 5.3: Two still images comparing methods to track the flow head within the device. Rhodamine B dye on the left and pink petal dust on the right. The petal dust appears grainy when compared to the dye.

A high-contrast dye was desired for visually analyzing the flow head in the devices. Rhodamine B[4] is a well-known, high contrast dye used in dye laser applications. In high concentrations it appears as a vibrant pink or magenta. It provides a stark contrast against any other color present in the experiment when viewed in person or through a camera.

Later, a pink petal dust was also tested as a different species for visualizing the flow head. Petal dust is a mica-based ultrafine powder that can be added to liquids to produce a pearlescent effect. The reason for testing a different colorant was because it was thought that the Rhodamine B was diffusing into the surrounding flow, thus making the shape of the flow head more blunted. This was based on the concurrent flow head analysis explained in Section 6. A suspended particle, like the petal dust, would not diffuse like a dye and theoretically give a truer

visualization of the flow. A number of trials were performed using a relatively high concentration of pink petal dust in place of Rhodamine B. Unfortunately, after testing the petal dust, it was found that it quickly fell out of suspension. Suspending the petal dust in glycerol kept the dust in suspension for slightly longer but it still crashed out to the bottom of the flow channel fairly quickly. The only way for the petal dust to stay suspended was to add a large amount of dish soap to the water as a surfactant. Due to the number of variables required to keep the petal dust in suspension, the petal dust was not used.

Liquid

Pure deionized water was used for most flow analysis runs. In later tests, various concentrations of glycerol were used to change the viscosity of the fluid. Concentrations from 60% to 10% glycerol by mass were tried in an attempt to limit the ability of the Rhodamine B to diffuse as it flowed (diffusion rate in a liquid is inversely proportional to its viscosity). However, it was found after many tests that adding glycerol increased the friction against the walls and changed the shape of the flow head.

A few other unsuccessful changes were made to the solvent to again attempt to limit the perceived diffusion of the dye. The water was saturated with NaCl to reduce diffusion. After testing it, however, it was clear that the salt started diffusing into the dye thus affecting the shape of the flow head. Petal dust was used, but for it to stay in suspension, a large amount of soap had to be added to the water (discussed prior). This kept it in suspension but affected the flow head immensely because the soap made the boundary of the water and edges of the channel a very different slip boundary condition compared to that of pure water. Namely the flow head did not

elongate as predicted or previously observed with water. After these tests, it was realized that deionized water was the best option.

Eventually, it was found that the dye did not diffuse fast enough to affect the flow head data. In addition, the chemical reactions would not diffuse like dye and spectroscopic data (Sections 7a and 8) of those reactions would not be affected by diffusion. Any minor diffusion was solved by changing the calculation multipliers in Section 7.

6 - Analysis of Experimental Flow Head

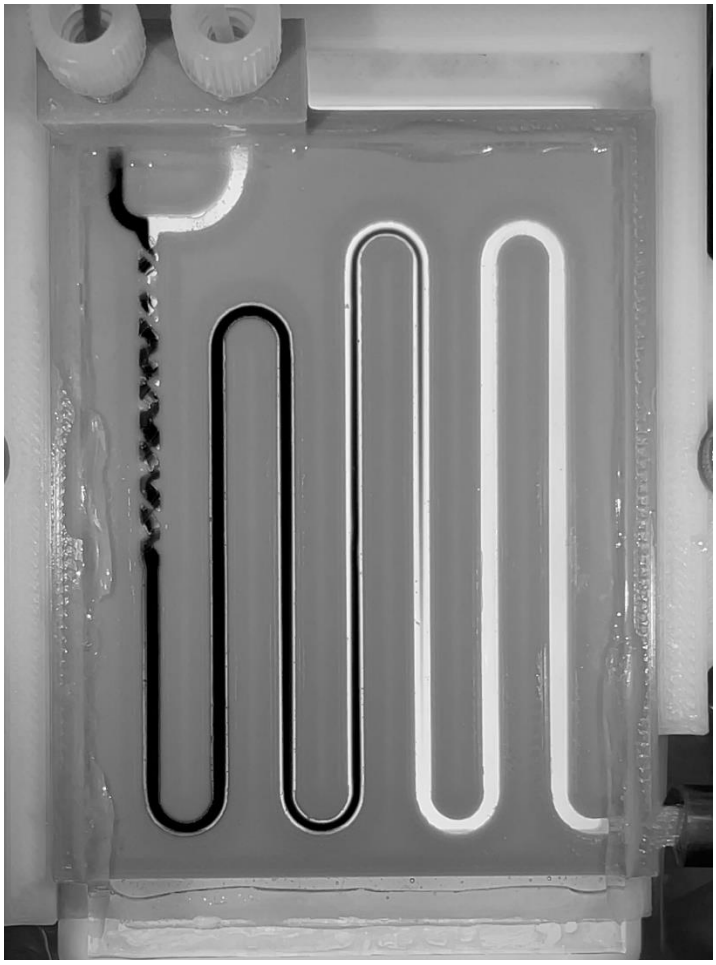

Figure 6.1: An image of the device digitally passed through a red/blue filter. The greyscale represents the intensity of green in the original picture. Lighter or white parts of the image represent a higher green pixel intensity and darker or black parts of the image represent an absence of green. Pink shows up black when viewed this way because pink is the complementary RGB color to green and is therefore the absence of green.

Flow analysis videos were taken on an iPhone 12 Pro's native camera app. Videos were shot in 4k at 60 frames per second and the camera's focus and exposure was fixed to the mixing region. The video files then had to be ingested and processed into readable data.

The first step of this process used Adobe Premiere Pro to export every thirtieth frame (i.e. half second snapshot) as a tiff file (a completely uncompressed file format) to retain all original pixels and their colors without compression. The folder of tiff files was imported into ImageJ, where the images were split into their red, green, and blue pixel values. This produced 3 separate image stacks that showed the value of a given color through grayscale (0-255; black-white). The blue and red image stacks were discarded because only the green values were useful for flow analysis with pink dye. Pink is the absence of green (i.e. the complementary color of green in the RGB color space), so with a green device and

a pink flow head, the device will appear as white or light gray (high grayscale values) and the pink dye will appear as black or dark gray (low grayscale values) as is shown in Figure 6.1.

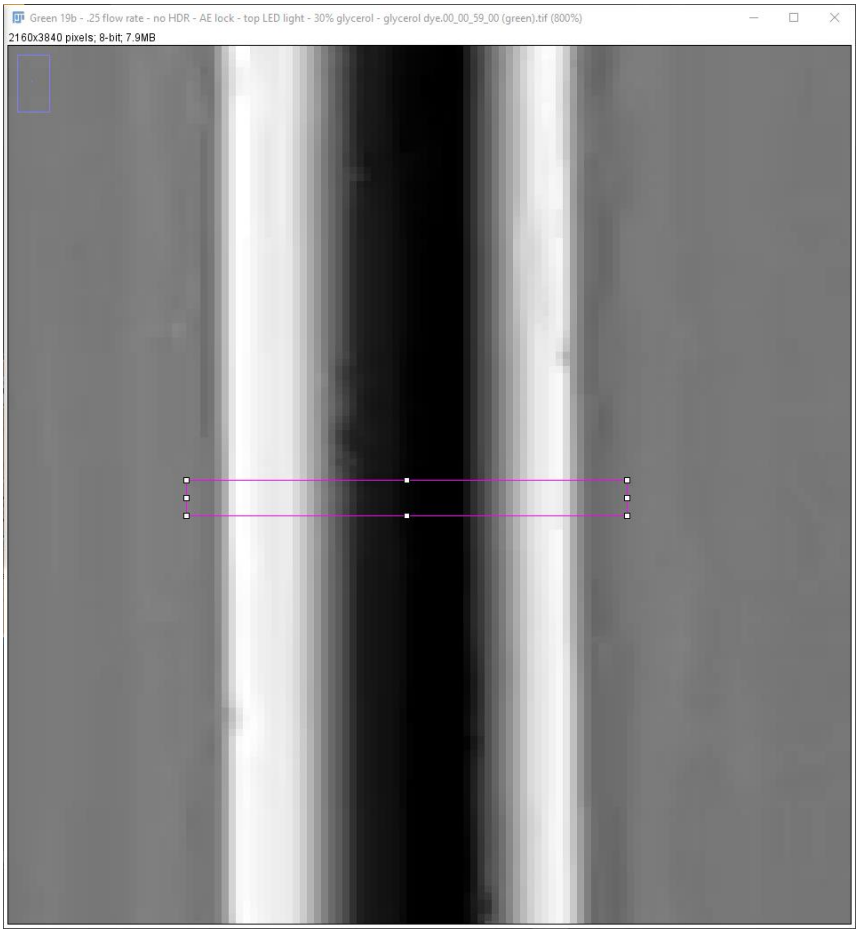

Figure 6.2: A highly magnified image of the flow head representing green intensity. (see Figure 6.1 for explanation) The magenta box is 5 pixels high and crosses the width of the channel. This box represents the values to be graphed in Figure 6.3. Pixel intensity values within the box are averaged by column to smooth the pixel results.

The image was zoomed in to be able to see individual pixels. A selection box was set to span the width of a given channel and 5 pixels in height. This box specified the pixels whose grayscale values were to be graphed by the program. ImageJ averages each column of green values then produces a graph. The graph is viewed for a single image (in the stack) where the flow head has not reached that section of the channel yet. A line was drawn across the graph where the channel appears white in the video. This was the baseline where the green value would be measured from. The edge of the pink dye flow head was specified to be the where the green value graph dipped below the line. The positions of the left and right sides of the flow head were recorded for each image in the stack allowing for the width of the flow head to be measured as a function of time.

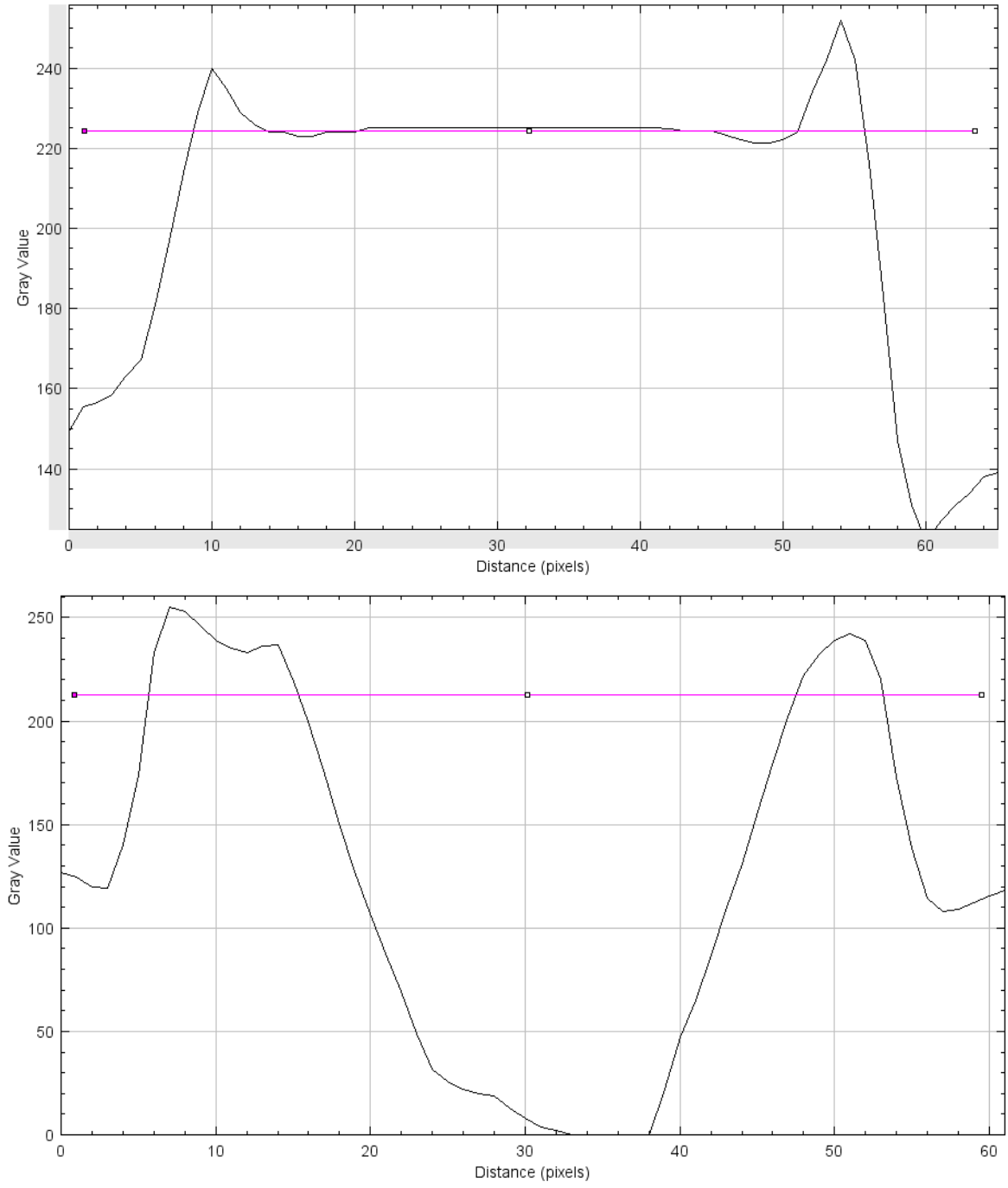

Figure 6.3: Two graphs representing the intensity of green in each pixel across the width of the channel. The top graph is of a section of empty channel that is filled with plain water and the bottom graph is of a section of channel where the dye flow head has partially passed through. The magenta line on the top graph was determined to be the value for an empty channel and was left in place to help determine the edge of the flow head as the dye passed through it. The edge of the flow head was said to be the inner bounds of where the magenta line intersects with the graph. The pixel width between the two peaks was said to be the width of the channel (to be used in later calculations).

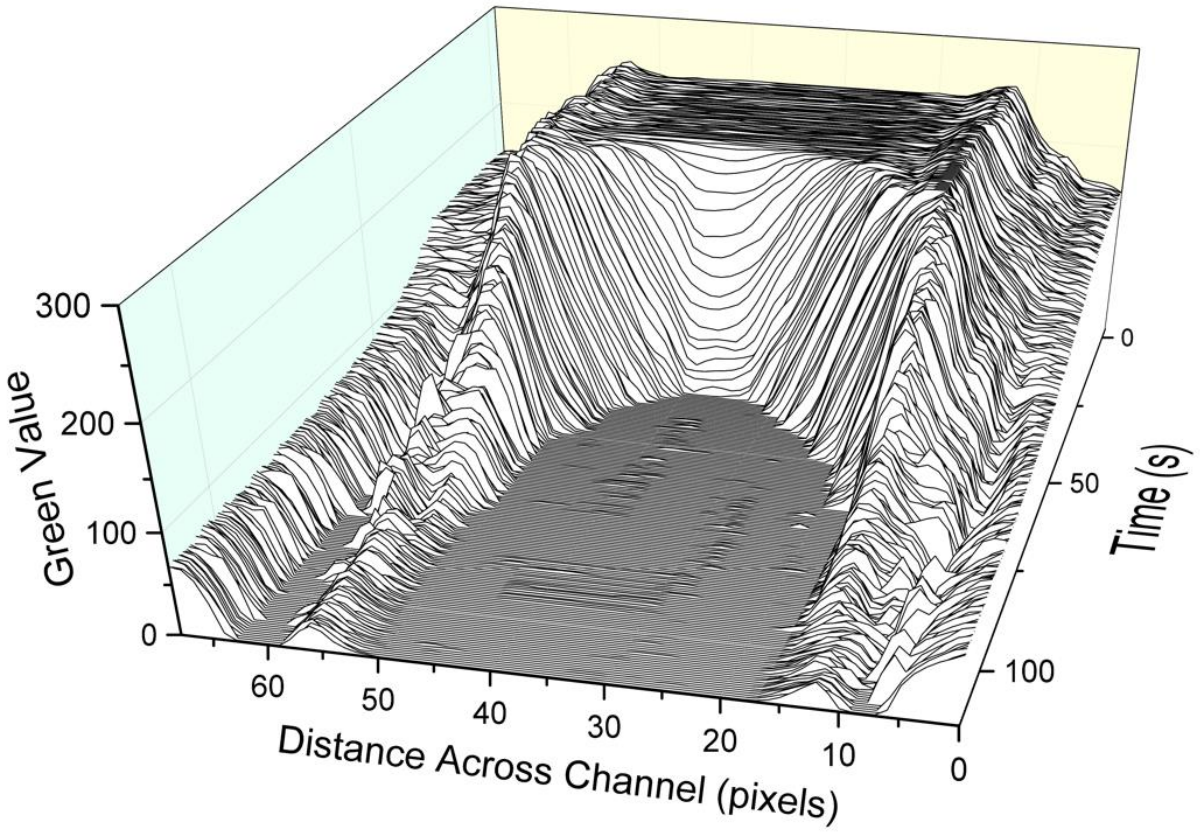

Figure 6.4: A 3D graph showing an initial test to visualize the flow head. The 3D graph is composed of the graph of green intensity across the width of the channel at every half second.

7 - Simulations in Excel

a. Velocity Calculator

The simulations in FLOW-3D were useful for visualizing the flow velocity distributions, but not for determining the precise curvature of the flow head. Fortunately, the velocity data could be used to calculate a more accurate version of the flow head. This secondary simulation was done using Excel. Velocity data from FLOW-3D was taken as a heatmap of the channel's cross-section. This data was then normalized into a flat velocity distribution grid. The numbers in each cell in the cross-sectional heat map were simply multiplied by the time the fluid had been in the device to produce a visualization of the flow head. The Excel calculator program displayed the shape of the flow head by approximation using 2D cross-sections at set points along the channel length. Each 2D cross-section had to summed into a 1D velocity distribution to represent what could be measured in the real-world experiment where the flow was viewed only from the top. These 1D slice representations were stacked together to represent an approximation of the flow head width at certain lengths down the channel.

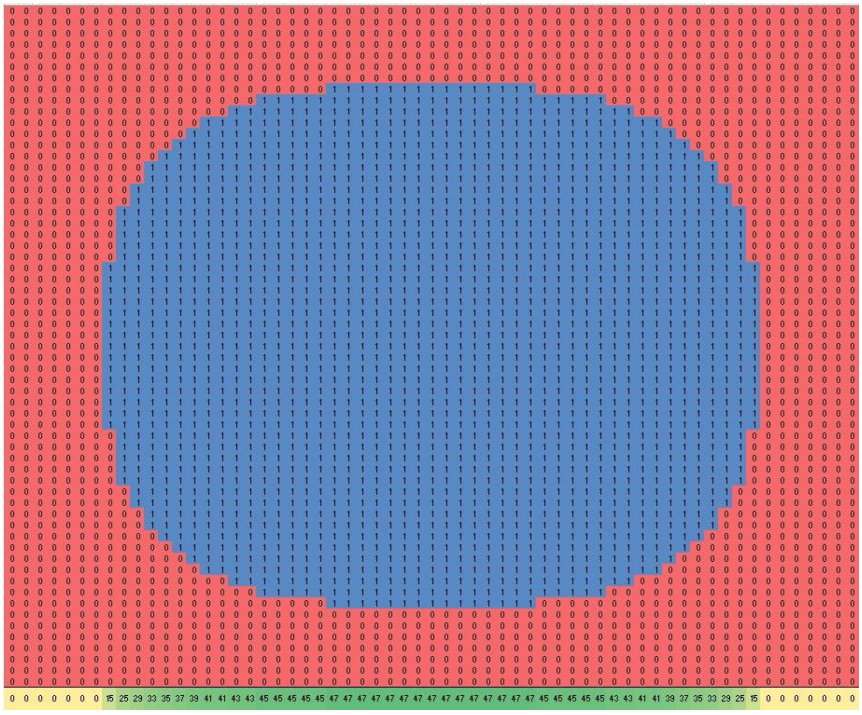

Figure 7.1: A single 2D cross-section of the simulated flow head. Red (0) indicates that the flow head is not present in that cell and blue (1) means that the flow head has passed through the cell. The row at the bottom is a sum of the 1s and 0s in each column. The summed row represents the top-down gradation seen in

The calculator uses two manual inputs: initial velocity and threshold. Initial velocity was the velocity the cross-sections were normalized to and the threshold represented the minimum value that the summed cells had to be for them to be considered at the "edge of the flow head". These could be varied to change the flow head shape to match the data from the real-world experiment.

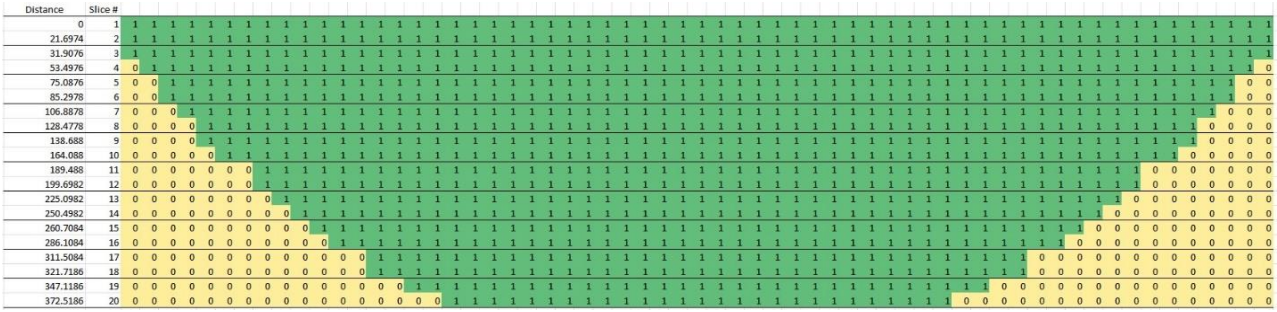

Figure 7.1: A combination of 20 summed cross-sections (see Figure 7.1) across the entire device. Each row represents one cross-section that has been passed through a threshold test. Green cells have been passed through by the flow head and yellow cells have not.

After many comparisons using different initial velocities and thresholds, it became abundantly clear that the FLOW-3D model was overestimating how slow the flow was at the walls of the channel. To correct for this the basic equation of the elliptical paraboloid was used ($f(x, y) = x^2 + y^2$) in conjunction with older experimental data to predict the curvature of the flow head. The outer values of the simulated flow data used to construct the flow head calculator were discarded so the curve would match much better to the experimental data. This corrected simulation data is what the Excel calculator program was originally based on.

	-0.7	-0.6	-0.5	-0.4	-0.3	-0.2	-0.1	0	0.1	0.2	0.3	0.4	0.5	0.6	0.7
-0.7	0.04	0.08	0.10	0.12	0.14	0.14	0.15	0.15	0.15	0.14	0.14	0.12	0.10	0.08	0.04
-0.6	0.08	0.18	0.26	0.31	0.35	0.38	0.39	0.40	0.39	0.38	0.35	0.31	0.26	0.18	0.08
-0.5	0.10	0.26	0.37	0.46	0.52	0.56	0.59	0.60	0.59	0.56	0.52	0.46	0.37	0.26	0.10
-0.4	0.12	0.31	0.46	0.57	0.65	0.71	0.74	0.75	0.74	0.71	0.65	0.57	0.46	0.31	0.12
-0.3	0.14	0.35	0.52	0.65	0.75	0.81	0.85	0.86	0.85	0.81	0.75	0.65	0.52	0.35	0.14
-0.2	0.14	0.38	0.56	0.71	0.81	0.88	0.93	0.94	0.93	0.88	0.81	0.71	0.56	0.38	0.14
-0.1	0.15	0.39	0.59	0.74	0.85	0.93	0.97	0.98	0.97	0.93	0.85	0.74	0.59	0.39	0.15
0	0.15	0.40	0.60	0.75	0.86	0.94	0.98	1.00	0.98	0.94	0.86	0.75	0.60	0.40	0.15
0.1	0.15	0.39	0.59	0.74	0.85	0.93	0.97	0.99	0.97	0.93	0.85	0.74	0.59	0.39	0.15
0.2	0.14	0.38	0.56	0.71	0.81	0.88	0.93	0.94	0.93	0.88	0.81	0.71	0.56	0.38	0.14
0.3	0.14	0.35	0.52	0.65	0.75	0.81	0.85	0.86	0.85	0.81	0.75	0.65	0.52	0.35	0.14
0.4	0.12	0.31	0.46	0.57	0.65	0.71	0.74	0.75	0.74	0.71	0.65	0.57	0.46	0.31	0.12
0.5	0.10	0.26	0.37	0.46	0.52	0.56	0.59	0.60	0.59	0.56	0.52	0.46	0.37	0.26	0.10
0.6	0.08	0.18	0.26	0.31	0.35	0.38	0.39	0.40	0.39	0.38	0.35	0.31	0.26	0.18	0.08
0.7	0.04	0.08	0.10	0.12	0.14	0.14	0.15	0.15	0.15	0.14	0.14	0.12	0.10	0.08	0.04

Figure 7.3: A table of the normalized velocity values by cell. These values were multiplied by the simulated time in the device to determine the distance the dye reached within each individual cross-sectional cell. Due to the flow at the edges of the channel in the FLOW-3D simulation not matching the experimental slip boundary conditions, the outer values were removed for all further calculations. This came from how the velocity at each mesh point is calculated and could

An initial central velocity was set and then a time value was input into the calculator. Each slice recalculates how many of the cells in that slice will have been passed through by the flow head. Stated another way, if the distance traveled by the flow head at a cell is larger than the slice's threshold distance (i.e. distance from the end of the mixing region to the slice), the cell is considered to have been passed through. If a cell has been passed through (i.e. has a faster velocity) then the cell is logged as a 1, if it has not been passed through it is logged as a 0 at that time increment.

Since the flow head was being viewed and measured from the top, only a 2D version of the flow head was observed experimentally. Therefore, all of the columns of 61 cells each for each slice are being viewed as a single value, not individual cells. The simulation adds up the values of the cells in each column to produce a 2D representation of the flow head from the simulation. This was done for each slice calculated. The time was then increased and the progression of the flow

through the device was mapped via many (usually 10 to 18) different slices at different positions within the device.

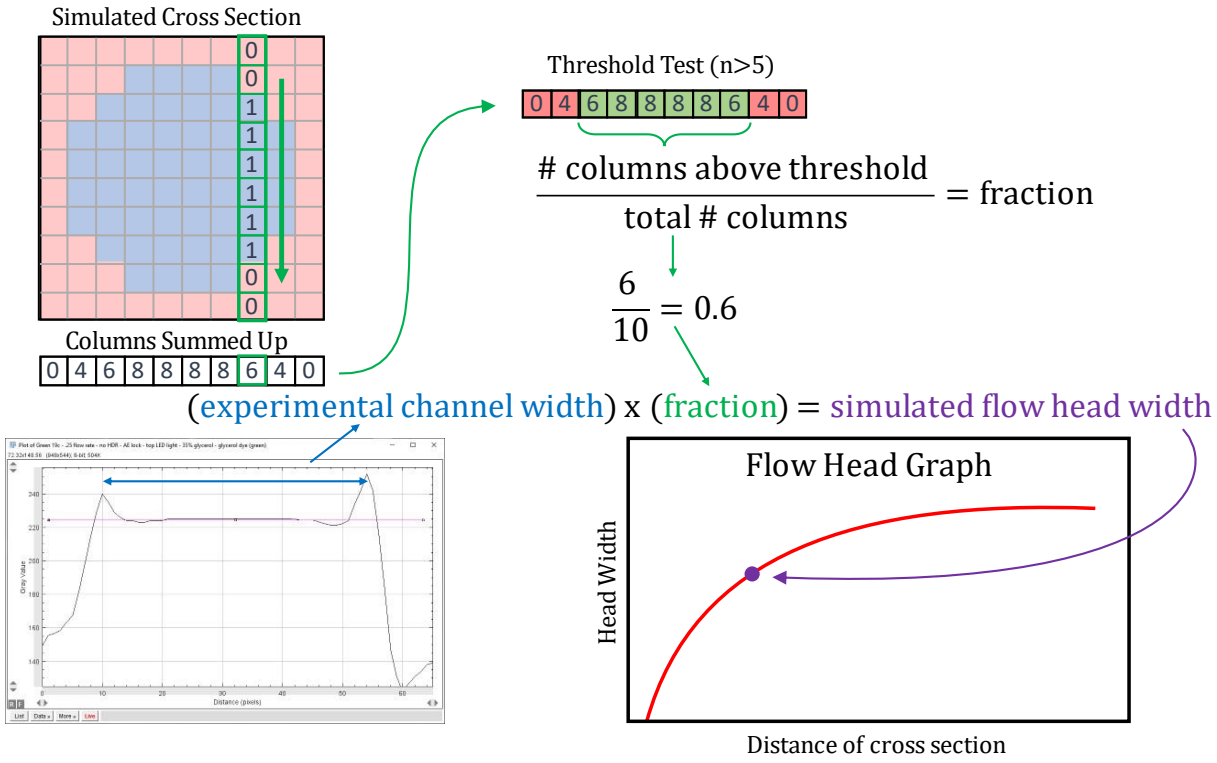

Figure 7.4: A diagram of how the velocity simulation within Excel, coupled with the experimental channel width, produced a single point on the flow head graph. Doing this many times produced a curve that could be compared with the experimental flow head curve.

A threshold distance was then chosen (corresponding to a particular distance of flow through the device) that was used to determine the 1s and 0s discussed previously. The evolution or elongation of the flow head through that threshold distance could then be simulated based on the fraction of columns that have had at least one of its cells achieve a value of 1. This fraction is therefore a value between 0 (no cells have passed through the slice) and 1 (at least one cell in each of the 61 columns of the slice has been passed through). The fraction could then be directly compared to the width of the green pixel values measured experimentally to gauge the level of agreement between the simulation and the observed flow progression.

The velocity calculations were run for long enough that the flow head would reach the end of the channel. The data it produced could be plotted and directly compared with the experimental spectroscopic data. The experimental data was plotted at each of 20 specified locations along the channel and the second-degree polynomial line of best fit was found. The x^2 value and constant from each of the locations' line of best fit was then averaged respectively. These two average values formed an average line of best fit for the specific experimental test. Many different experimental tests were run and the best were selected (by lowest error and best consistency) to be used for the spectroscopy simulation's parameters.

b. Spectroscopy Simulation

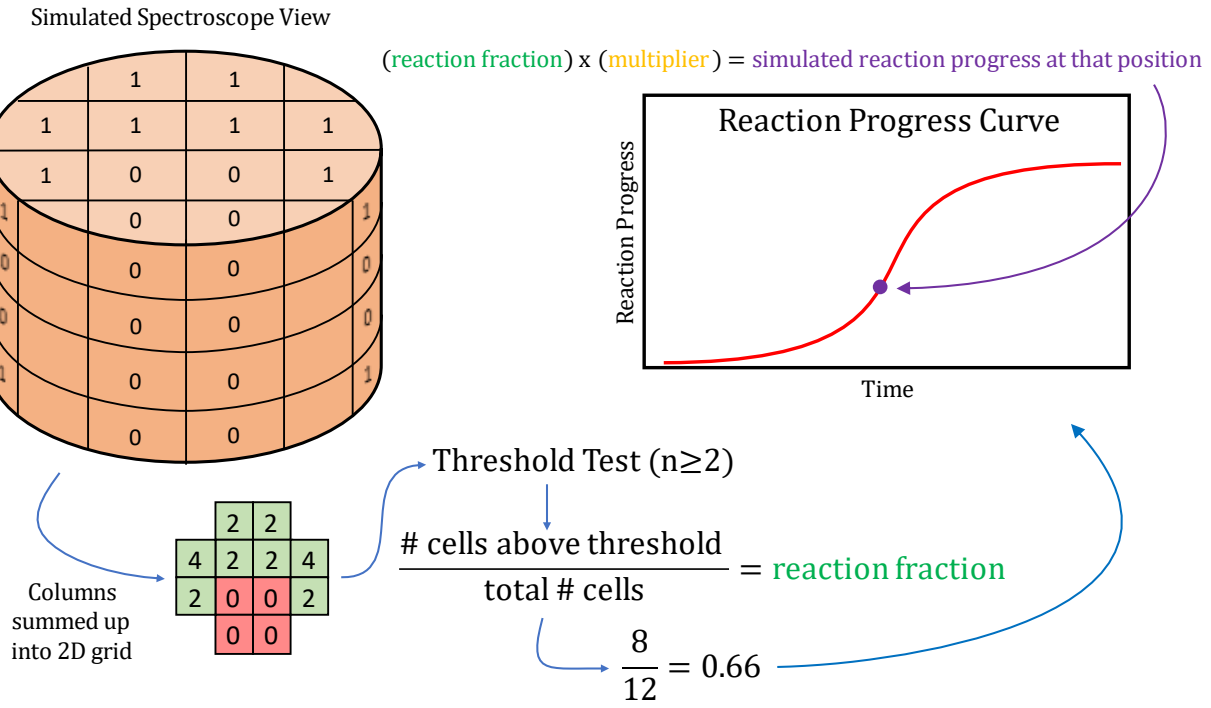

Figure 7.5: A low-resolution diagram of how the spectroscopy simulator within Excel produced a reaction progress curve. The 3D approximation of the cylinder was summed up by column and passed through a threshold test to get the fraction of cells within the simulated spectrometer's view that had reacted. Doing this for many time increments produced a curve that could be directly compared with previously measured spectral data.

After a more accurate set of velocity data was determined from the velocity calculations, it was used to make an absorbance spectroscopy simulator. The velocity data came in the form of a heat map of relative velocities for each cell within a cross-section of the device. This had to be used to calculate reaction time and position of a flow head so the expected absorbance spectra of a chemical reaction could be simulated and compared to previously measured spectroscopic data.

The velocity could be used to locate the position of the flow head at any given time. This was as simple as multiplying the velocity heatmap by the time the liquid had been flowing for. The problem with this method was that this was supposed to simulate a reaction and not simply a

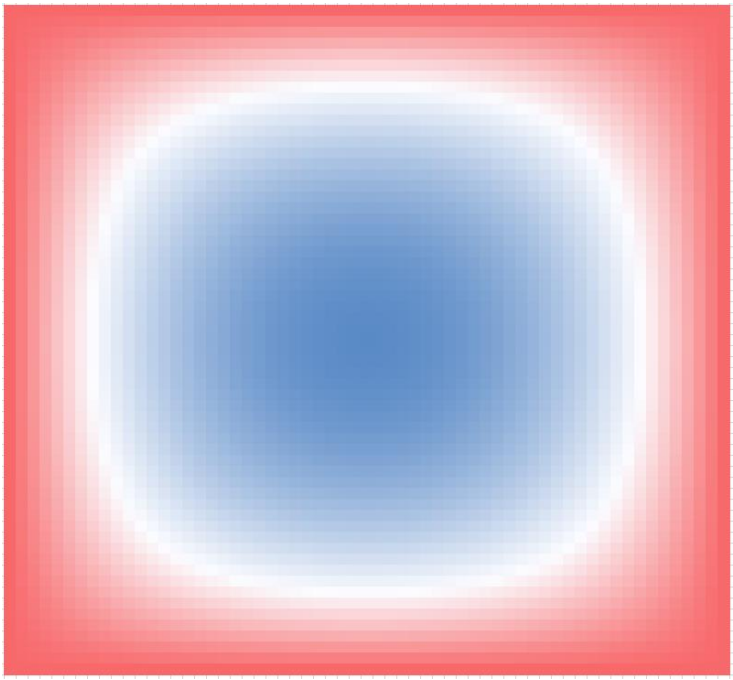

Figure 7.6: A high-resolution heat map of the velocity within a single cross-section of the device. Blue indicates that the cell is moving faster and red indicates that the cell is moving more slowly.

moving flow head. Reactions progress over time, but the reaction was also flowing through the device at the same time. With an input distance, rather than an input time, the reaction progress (elapsed reaction time) could be calculated. The simple physics equation correlating distance and time (Section 1) formed the backbone of the spectroscopy simulation program.

The previous spectra that are being compared are based on what is known as a clock reaction. Once the reactants are mixed, there is a predicable delay in the formation of the products. The reaction previously studied was a version of the classic iodine clock reaction where the initial reactants are clear and, after a pre-determined delay time, the vibrant blue product forms. To account for this delay time in product formation, and thus absorbance measurements in the previous

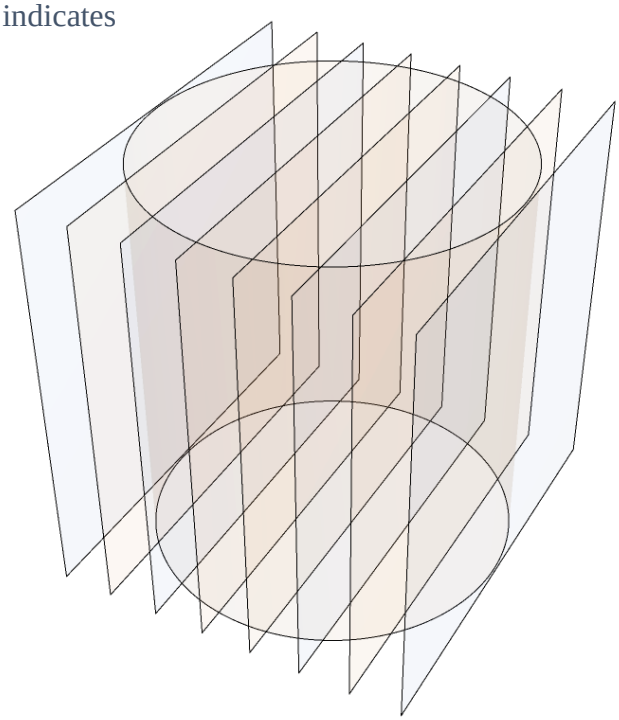

Figure 7.7: A depiction of how the simulated spectroscopic view was approximated. The cylinder was divided into slices whose width was then approximated with cells. Essentially this divided up the cylinder into a collection of cubes which could then be summed and calculated in 2D.

spectra, the simulated reaction data had to be passed through a numerical filter. The filter essentially ignored time values under a certain predefined reaction threshold.

Slice	Offset Dist																									
1	-0.3														16											
2	-0.275							18	18	16	16	16	16	16	16	16	18	18								
3	-0.25					18	18	18	18	16	16	16	16	16	16	16	18	18	18	18						
4	-0.225				20	18	18	18	18	18	16	16	16	16	16	18	18	18	18	18	20					
5	-0.2			20	20	18	18	18	18	18	16	16	16	16	16	18	18	18	18	18	20	20				
6	-0.175		22	20	20	18	18	18	18	18	16	16	16	16	16	18	18	18	18	18	20	20	22			
7	-0.15		22	20	20	18	18	18	18	18	16	16	16	16	16	18	18	18	18	18	20	20	22			
8	-0.125	22	22	20	20	18	18	18	18	18	16	16	16	16	16	18	18	18	18	18	20	20	22	22		
9	-0.1	22	22	20	20	18	18	18	18	18	16	16	16	16	16	18	18	18	18	18	20	20	22	22		
10	-0.075	24	22	22	20	20	18	18	18	18	18	16	16	16	16	16	18	18	18	18	18	20	20	22	22	24
11	-0.05	24	22	22	20	20	18	18	18	18	18	16	16	16	16	16	18	18	18	18	18	20	20	22	22	24
12	-0.025	24	22	22	20	20	18	18	18	18	18	16	16	16	16	16	18	18	18	18	18	20	20	22	22	24
13	0	24	22	22	20	20	20	18	18	18	18	16	16	16	16	16	18	18	18	18	20	20	20	22	22	24
14	0.025	24	22	22	20	20	20	18	18	18	18	16	16	16	16	16	18	18	18	18	20	20	20	22	22	24
15	0.05	24	22	22	20	20	20	18	18	18	18	16	16	16	16	16	18	18	18	18	20	20	20	22	22	24
16	0.075	24	22	22	20	20	20	18	18	18	18	16	16	16	16	16	18	18	18	18	20	20	20	22	22	24
17	0.1		22	22	20	20	20	18	18	18	18	16	16	16	16	16	18	18	18	18	20	20	20	22	22	
18	0.125		22	22	20	20	20	18	18	18	18	16	16	16	16	16	18	18	18	18	20	20	20	22	22	
19	0.15			22	20	20	20	18	18	18	18	18	16	16	16	18	18	18	18	18	20	20	20	22		
20	0.175			22	20	20	20	18	18	18	18	18	16	16	16	18	18	18	18	18	20	20	20	22		
21	0.2				20	20	20	18	18	18	18	18	16	16	16	18	18	18	18	18	20	20	20			
22	0.225					20	20	18	18	18	18	18	16	16	16	18	18	18	18	18	20	20				
23	0.25						20	18	18	18	18	18	16	16	16	18	18	18	18	18	20					
24	0.275							18	18	18	18	16	16	16	18	18	18	18								
25	0.3												16													

Figure 7.8: The view of the simulated spectrometer (colored for ease of visualization). Green indicates columns that have reacted less and red indicates columns that have reacted further. The value of each cell in this view is averaged to simulate the value the experimental spectrometer would graph.

The simulation had to recreate a view of the flow through the channel from only the field of view that the spectrometer had. This meant making a cylinder from a number of the previously used slices. This required reducing the circle of the cylinder to a grid estimation of the circle as viewed from the top. A centerline was defined to be the diameter of the circle perpendicular to the walls of channel. Cross-sections of the cylinder were taken at set intervals (positive and negative)

from the centerline across the width of the cylinder to essentially represent it in a 3D grid. A distance could now be defined which would move the center of the simulated spectrometer to match up with the position of the experimental spectrometer used to collect any specific plot of data.

The simulated spectroscopic data was run using varying velocity data produced by the different experimental averages from the velocity calculator. Approximately 25 different spectroscopy simulation data sets were considered and compared to the experimental spectroscopic data. The best was then selected and was determined to be the most accurate to use for further simulations.

The final results were determined as accurate to the set of spectral data from a single test of the iodine starch reaction. This data might later be optimized better with many tests and a larger data set to average. For now, this simulation data matches the experimental data enough to move forward knowing this calculator can be used to predict spectral data before running the experiment.

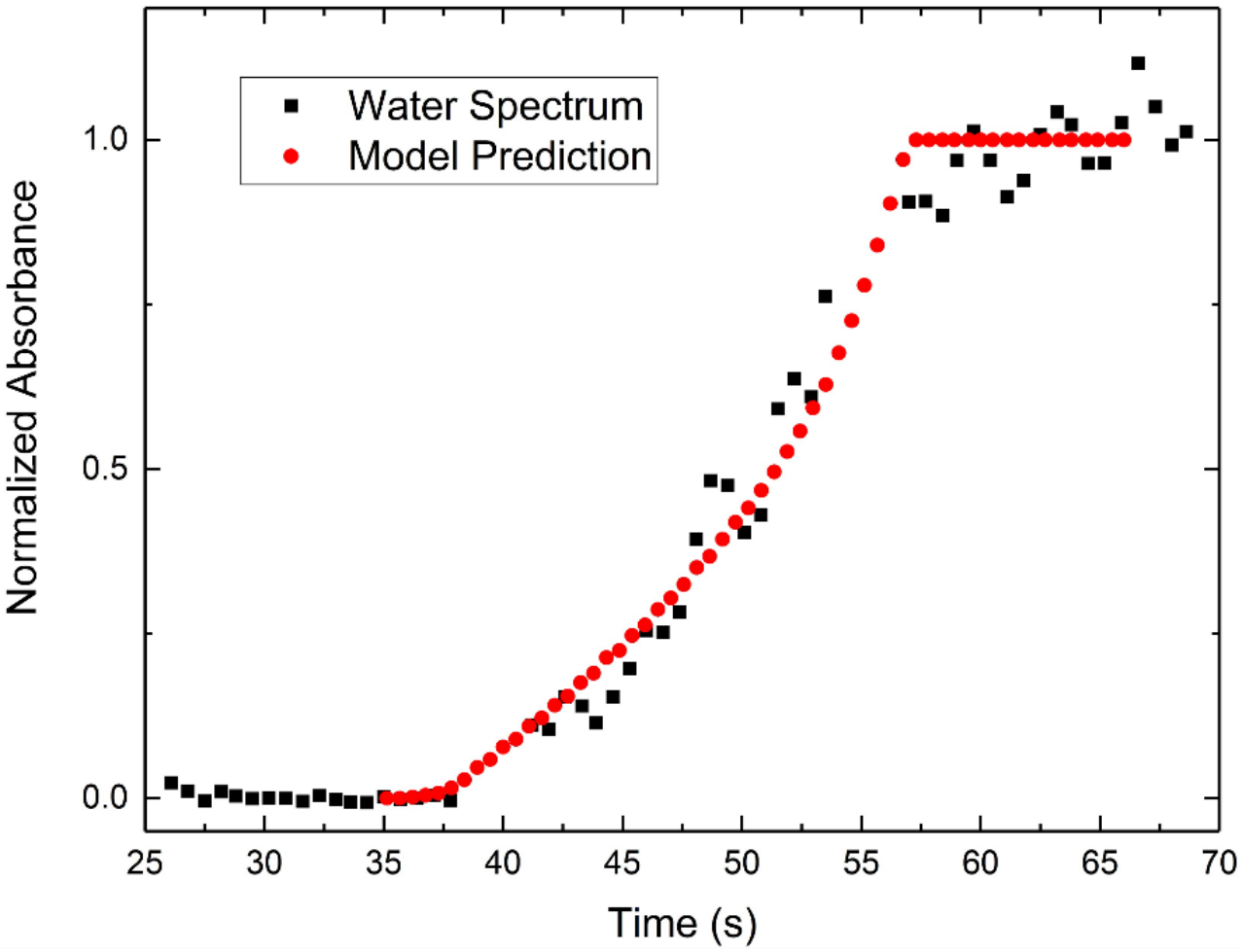

Figure 7.9: A graph comparing the experimental absorbances of the iodine starch reaction to the simulated spectrum. This simulated curve was found to be the most accurate to the experimental data.

8 – Conclusion and Further Research

Over the course of this work a number of things were confirmed and refuted regarding the nature of the flow in the 3D printed millifluidic devices. The flow is indeed laminar and generally adheres to the expected principles of laminar flow dynamics with a partial-slip boundary condition (not the more ideal and expected no-slip boundary condition). The laminar nature of the flow is consistent throughout the device and the shape of the flow head is predictable as an elliptical paraboloid. Results of some of the previously acquired data on the iodine clock reaction were able to be accurately reproduced using the velocity model developed by this project.

Going forward, this work will be used to try to decouple the flow dynamics from the actual kinetics present in a chemical reaction. If possible, this decoupling will allow for measurements of kinetic quantities, such as rate constants, for evolving reactions and will open up possibilities for future studies utilizing these devices.

References

1. Morley, S.E., Knurr, B.J., Probing the Role of the Solvation Shell for the Iodine-Starch Complex using Millifluidic Devices, J*ournal of Solution Chemistry*, 2021, 50, p 833–850

2. *FLOW-3D*® Version 12.0 [Computer software]. (2019). Santa Fe, NM: Flow Science, Inc. https://www.flow3d.com

3. Engineering ToolBox, (2003). Reynolds Number. https://www.engineeringtoolbox.com/reynolds-number-d_237.html (Dec 12, 2022).

4. Rhodamine B Citation: Smart, P.L., Laidlaw, M.S., "*An Evaluation of some Fluorescent Dyes for Water Tracing*", Water Resource Research, 1977, 13, p 15-33